The International Journal of Advanced Manufacturing Technology (2023) 127:625–634
https://doi.org/10.1007/s00170-023-11587-8

ORIGINAL ARTICLE

Qualify a NIR camera to detect thermal deviation during aluminum WAAM

Anthony Dellarre[1] · Nicolas Béraud[1] · Nicolas Tardif[2] · Frédéric Vignat[1] · François Villeneuve[1] · Maxime Limousin[1]

Received: 7 February 2023 / Accepted: 11 May 2023 / Published online: 16 May 2023

Abstract

This paper proposes to qualify the minimal quality deviation that can be detected by a near-infrared camera during aluminum wire arc additive manufacturing. First, a review of the literature is done to highlight the interest in monitoring the melt pool in industrial condition for thermal management during manufacturing. It points out the relevance of the use of a near-infrared camera for steels, but it has to be demonstrated for aluminum alloys. Indeed, the melt pool of the aluminum is significantly dimmer and less distinct than the melt pool of the steels. An experimental design is proposed to qualify the minimal quality deviation that can be detected on a thin wall. The chosen default to correlate with the thermal deviation is the width of the wall. A method is proposed to extract a thermal metric from the camera image and to analyze its sensitivity to a width deviation of the wall. The paper shows the correlation between the width of the wall and the thermal metric for different heat conditions. Moreover, the thermal metric is sensitive to width deviation either on the wall scale or on the bead scale. It indicates the relevance of a near-infrared camera to detect heat accumulation-induced width deviation during wire arc additive manufacturing of aluminum alloy.

Keywords Wire arc additive manufacturing · Near-infrared camera · Thermal monitoring · Defect detection · Aluminum alloy

1 Introduction

Wire arc additive manufacturing (WAAM) is a direct energy deposition process. It is composed of an electric arc heat source moved by a computer numerical control machine or a robot. The torch deposes a metallic bead on a substrate, and the stacking of the beads creates the part [1]. Many heat sources are available for the modulation of the input energy and material [2]. The gas metal arc welding (GMAW) associated with cold metal transfer (CMT) technology is one of these solutions. It allows a high-rate material deposition and a better energy control. Any material that can be welded can be used in WAAM.

Nevertheless, this technology faces with several challenges [3, 4]. Multiple defaults can be observed during manufacturing, such as porosity [5, 6], residual stress [7, 8], dimensional defects [9, 10], and microstructure [11]. The defects do not have the same intensity in function of the chosen material [12]. However, most of these defects results from poor heat management during manufacturing [13]. Thus, managing heat during the manufacturing is a key challenge for the development of the technology.

The literature proposes some tools to mastering these effects [14]. Empirical methods can be set up. The result of the experiment can lead to establish abacus or manufacturing rules [15]. Another solution is to simulate the process in order to define optimal manufacturing parameters that can be defined for an open loop [16]. Moreover, closed-loop control is an effective method to control the process [17]. Developing pertinent sensors for in-operando monitoring to closed-loop control is the subject of many papers [18]. Nevertheless, there is lacking in the literature of a metric to monitor in industrial condition during production, especially for aluminum alloys.

Several thermal metrics can be monitored during the process (temperature on a point, temperature field, and substrate temperature). The evolution of the melt pool may be

✉ Anthony Dellarre
anthony.dellarre@grenoble-inp.fr

[1] Institute of Engineering, Univ. Grenoble Alpes, Grenoble INP*, CNRS, G-SCOP, 38000 Grenoble, France

[2] Lamcos, INSA Lyon, Université de Lyon, CNRS, Villeurbanne, France

a good metric to capture the heat accumulation responsible for most of the defects [19]. Different devices are proposed in the literature to measure the melt pool. A combination of laser light and a camera with the corresponding band-pass filter can obtain the shape of the melt pool. It is possible to observe it through the electric arc [20]. Another physical value which can be obtained is the thermal field of the melt pool using a microbolometer [21]. These devices are large and create a large quantity of data. They are appropriate to understand physical phenomena but not to monitor a metric of the melt pool for control. The device must allow the machine to work in industrial condition.

An interesting solution is to use an industrial near-infrared camera such as CMOS (complementary metal-oxide semiconductor) or CCD (charge coupled device) camera. It is sensitive to visible and near-infrared light radiation (wave lengths from 400 to 1100 nm). It is consistent with the radiation spectrum emitted by the melt pool [22, 23]. Dimensional metrics such as length, width, or surface of the melt pool can be extracted from the field measurement. These devices are compact and easy to implement in industrial conditions, but the information is restrained to global phenomena. Conclusive results are obtained with steels due to the good sensitivity of the sensor in such conditions. Numerical method can be used like Canny filters or adaptative threshold to automatically detect the melt pool and extract a metric from the melt pool. Nevertheless, the adaptation of this method to aluminum alloys is more challenging. Indeed, the thermal emission light of the melt pool is 1000–10,000 times lower than steel, and the melt pool boundary is less distinct [24]. Figure 1 illustrates the difference between two raw images taken from aluminum alloy and steel manufacturing.

Since thermal deviation is assumed to be responsible for most of the defects, this paper investigates the use of a monomodal instrumentation to capture the deviation of a thermal metric using a near-infrared camera. The main challenge is to determine how to qualify the minimal quality deviation that can be detected by a near-infrared camera during aluminum wire arc additive manufacturing processes. This qualification is studied on two scales: on the scale of a wall and on the scale of a bead. In the present work, the defect to be correlated is the width deviation. Indeed, to produce functional part, the first defect to master is the geometry accuracy. As the geometry is linked to the thermal conditions [26], the bead does not have the same width in function of the heat accumulation. A correlation between the width and a metric of the melt pool measured with the CMOS camera is sought.

First, an experiment is proposed to estimate the smallest quality deviation detected by the device. Walls with different thermal conditions are built. The post-processing of the images taken in-operando enables to extract a thermal metric related to the area of the melt pool. The thermal metric is compared to local width measurement of the layers of the walls to estimate the minimal deviation that can be captured. Finally, the analysis of the result allows highlighting the interest to monitor a metric of the melt pool for heat management during manufacturing on the time scale of the camera acquisition.

2 Materials and methods

2.1 Experimental design

Thin walls are manufactured and filmed using a near-infrared camera to monitor the area around the melt pool with a side view angle. The manufacturing technology is mature enough to make straight thin walls by controlling the thermic. Indeed, an idle time between layers is commonly used to control the thermal accumulation [27]. Two walls are manufactured: one with a short idle time of 2 s where a large heat accumulation can be observed and another with an idle time of 30 s where a little heat accumulation can be observed. Images are taken in-operando with the near-infrared camera. From these images, a thermal metric is extracted. After manufacturing, each wall is measured with a 3D scan to extract the width deviation in function of the layer and the longitudinal position.

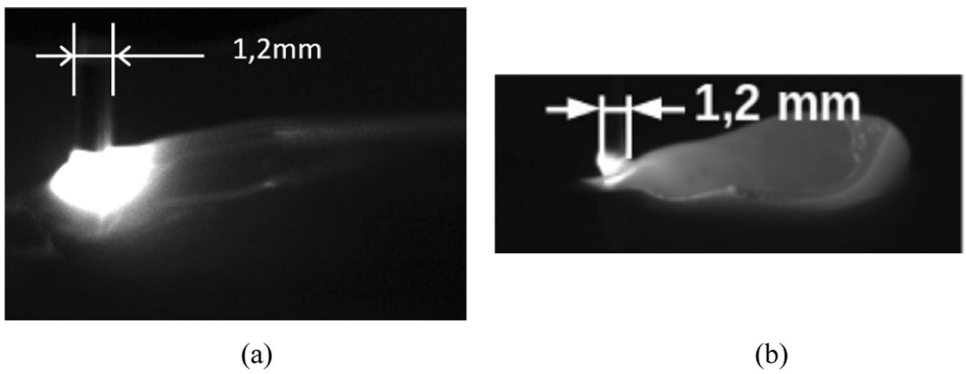

Fig. 1 Comparison of the melt pool image measured with a CMOS camera in function of the material, **a** aluminum alloy [24], and **b** steel [25]

Table 1 Manufacturing parameters

Material	Wire diameter	CMT law	WFS_S	TS	Layers	Wall length	Delta z per layer	Idle time between layers	Deposition strategy
AlMg3Cr	1.2 mm	875	4 m/min	40 cm/min	42	150 mm	2.3 mm	2 s or 30 s	Zigzag

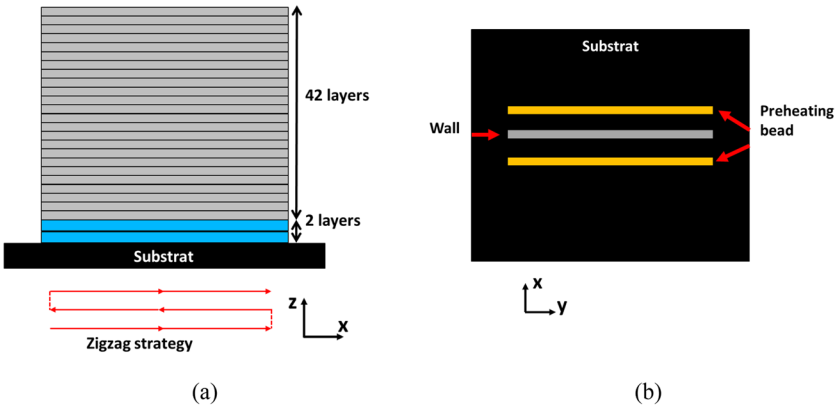

Fig. 2 Manufacturing strategy: **a** side view and **b** top view

The width and the thermal metric are compared on two scales. First, the thermal deviation is qualified on the wall scale. on this scale, the ends of the wall are not studied because their thermal conditions are particular. The data from the geometrical scan and the thermal metric are truncated, averaged, and compared. Then, the thermal deviation is qualified on the bead scale. In this case, all the data of the layer are kept. The thermal particularity of the ends of the wall allows quantifying the sensitivity of the device.

2.2 Experimental set up

2.2.1 Manufacturing conditions

The WAAM machine is composed of a 6-axis robot, Yaskawa MA1440, and a positioner with 2 axes and a welding station, Fronius T.P.S. CMT 4000 Advanced. The material is an AlMg3Cr alloy. The wall is 150 mm long, and it is composed of 44 layers. It is built on a 250 mm * 250 mm * 5 mm aluminum plate in AlMg3 at an initial temperature of 60 °C.

To improve the initial thermal conditions, 2 beads are deposited on each side of the wall, at 20 mm, with a 30-cm/min robot travel speed (TS) and a 6.1-m/min synergic wire feed speed on the RCU (WFS_S). Then, the first 2 layers of the wall are deposited with a TS of 30 cm/min and a WFS_S of 5 m/min with a zigzag strategy. Finally, 42 layers are deposited with a zigzag strategy and the chosen idle time with the parameters presented in Table 1. Figure 2 illustrates the deposition strategy.

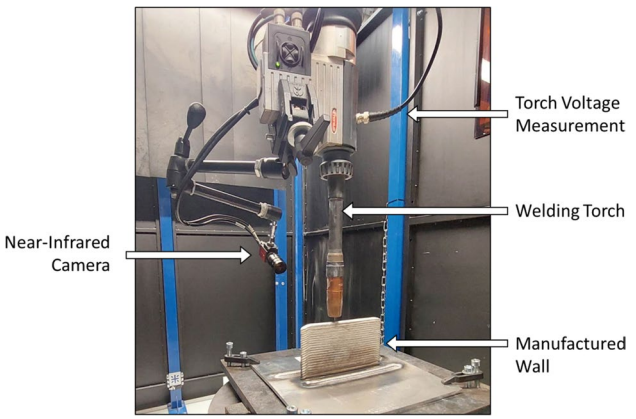

Fig. 3 Camera fixation on the torch

2.2.2 In-operando measurement of the melt pool

The CMOS camera is a Mako G-040B monochromatic with a Kowa LM35JC lens (focal of 35 mm). To measure the melt pool in-operando, the CMOS camera is fixed on the welding torch to maintain a constant distance between the camera and the robot-driven tool center (Fig. 3). Figure 4 illustrates typical image obtained with the camera.

The welding process used for this experiment is based on a CMT law. In this case, the welding station produces a periodic electric arc with an approximate period of 10 to 20 ms. Images are taken when the electric arc is off. Indeed, that avoids images saturated by the electric arcor by the emission of the plasma of the shield gas masking the thermal emission of the melt pool.

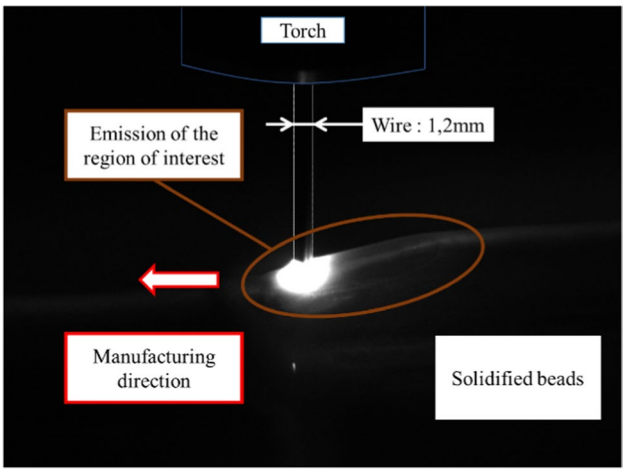

To trig the camera, a zero-voltage detection is necessary, which corresponds to the stop of the electric arc. Then, the image is taken after a delay. If the delay is too short, a residual plasma around the melt pool deteriorates the image for analysis (Fig. 5a). If the delay is too long, there is not enough time to take the image with the correct exposure time (Fig. 5c). Empirically, the delay is set to 1.2 ms and the exposure time to 0. 5ms considering that the short-circuit time is approximately 2 ms (Fig. 5b). Considering that a CMT cycle has an approximate duration of 10 to 20 ms, an idle time of 100 ms is set after a trigger to limit data (Fig. 6). Thus, the acquisition frequency is around 8 Hz, and this means approximately one image every 5 electrical arcs. The camera configuration is summed up in Table 2.

Fig. 4 Typical image obtained with the NIR camera

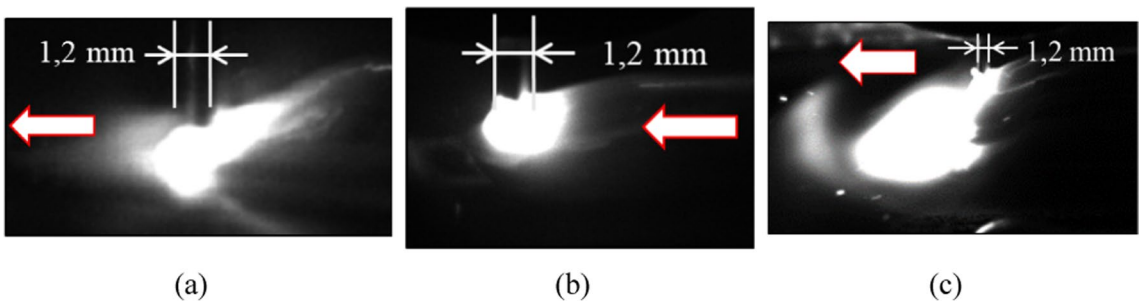

Fig. 5 Example of image function of the delay and the exposure time. **a** shorten delay, **b** a correct image, and **c** an image with too much delay or exposure time

Fig. 6 Trigger temporality

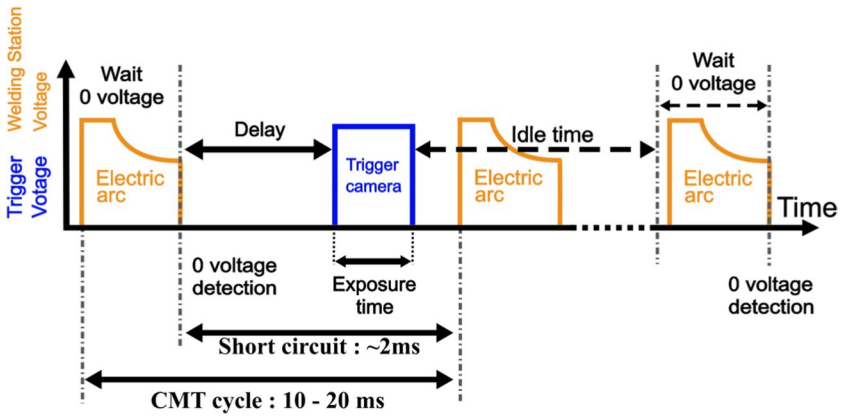

Table 2 Camera configuration

Camera	Frame per second	Exposure time	Trigger delay	Idle time	Gain	Resolution	Bit depth	Objective	Focal
Mako G-040B	~ 8	0.5 ms	1.2 ms	100 ms	22	728 × 544	8	KOWA LM35JC	35 mm

2.2.3 Measurement of the geometrical deviation

When the wall is built, the shape of the wall is obtained using a structured-light 3D scan. The GO!SCAN SPARK™ has been used. Its accuracy is up to 0.05 mm, with a mesh resolution of 0.5 mm. Using the VXelements software, the point cloud is filtered and exported as an STL file.

2.3 Data processing

2.3.1 Image processing

The aim of the image processing is to automatically obtain a thermal metric from the captured image.

Images are taken during the process, and a metric is extracted automatically. To exacerbate the light intensity, an image process is used [24]. A logarithm is applied to each image. Then, a threshold at 45% of the bit depth of the image is applied. All values under this threshold are set to 0, and the others are linearly distributed (Fig. 7).

There is a numerical trigger, because there are some images that have too many perturbations. This disturbance may be due to projections. The projection illuminates the wall which is more luminous than the melt pool (Fig. 8a). It may also be due to a shorter circuit. The end of the exposure time of the image is illuminated by the beginning of the electric arc (Fig. 8b). To sort out these images, the mean intensity of each image is calculated, and a histogram is plotted in function of the percentile of the mean image intensity of the sample (Fig. 9). The first 5% of the lower intensity images and last 20% of the higher intensity images are excluded, because their characteristics are clearly different from those of the other images of the sample.

Last, a thermal metric of the process zone is extracted using the python library OpenCv [28]. All the images are

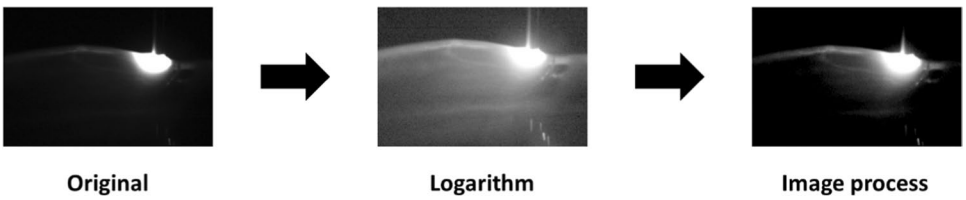

Fig. 7 Image process

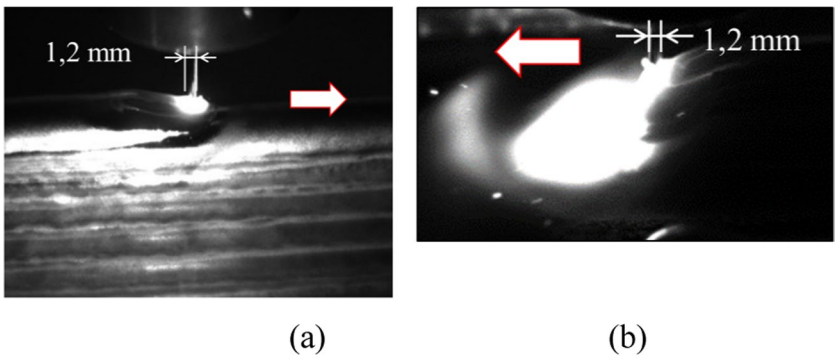

Fig. 8 Examples of perturbation on the images. **a** Due to projection and **b** due to shorter circuit

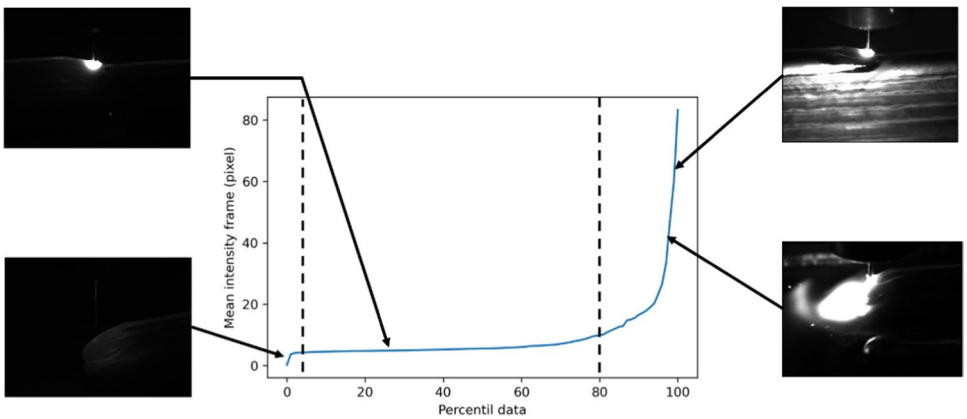

Fig. 9 Percentile exclusion

monochromatic with a bit depth of 8. First, a binary threshold is applied with a value equal to 100. A morphological closing is applied to the output of the threshold with 4 × 4 one kernel. The biggest white spot (value of 1) is kept (Fig. 10). This spot is called the thermal processed area, and its surface is called the thermal metric. Then, the images are labeled with the layer number.

The thermal metric obtained is different from the melt pool. Filters such as canny or adaptative threshold, usually used to get the boundary of the melt pool for alloys with higher solidus temperature, do not give expected result for aluminum alloys. However, as the contour made with the binary threshold is linked to the thermic, a correlation between the value of the thermal metric and the melt pool can be expected.

2.3.2 Scan process

The goal of the scan process is to obtain a map of the wall width as a function of the layer and the x-axis.

First, the STL file is imported using GOM Inspect 2018. A new basis is defined by the wall in the x direction and the vertical is on the z-axis (Fig. 11). The wall is sliced along the x-axis every millimeter. One hundred and fifty-one slices are created. These slices are exported as 151 2D $(\vec{y}, \vec{z})$ point clouds.

For each slice, only the left and right sides of the wall are kept. Points from the plate or the top surface (2.3 mm under the highest point) are deleted. Moreover, the 6th first beads are not considered (6 × 2.3 mm = 13.8 mm). The least mean square line of the point cloud is calculated. It represents the middle plan of the wall in the current slice. For each point, the normal distance between the point and the line is calculated, corresponding to the half wall thickness (Fig. 11). That allows plotting the wall thickness as a function of the wall elevation. Considering the layer surface constant for each layer, the width and height of each layer as a function of the x-coordinate are determined.

2.4 Online material

The data generated during each experiment is available with the creative commons license CC BY-NC 4.0. The raw images, the scan on STL format, the thermal metric shortened by layer, and the geometry of the bead function of the layer and its x coordinate are shared [29].

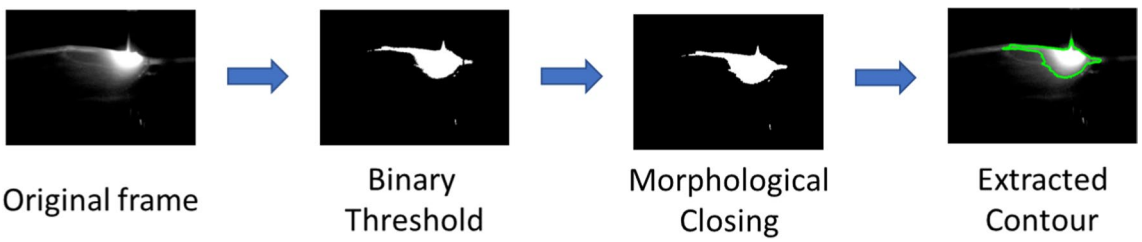

Fig. 10 Image process for metric measurement of the image

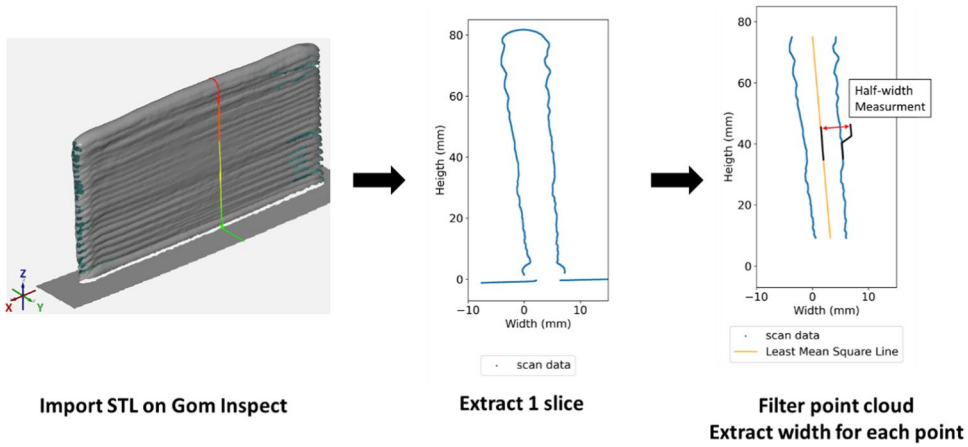

Fig. 11 Width extraction method

3 Result

3.1 On the wall scale

For this result, data from the ends of the wall are excluded. The first 20 mm and last 20 mm of each layer of the scan are then not considered, which correspond to the first 13% and last 13% of the thermal metric for each layer. The mean value of the width and the thermal metric is calculated for each layer. The first 6 layers are not considered. The 7th layer is considered the reference. The deviation of the width and the thermal metric are calculated in percent for each layer to the referent layer (layer 7). The deviation is defined by Eq. (1). Results are presented in Fig. 12:

$$Deviation(layer\_I) = \frac{X(layer\_I) - X(layer\_7)}{X(layer\_7)} \times 100 \quad (1)$$

3.1.1 Idle time of 2 s

The reference width (layer 7) is equal to 5.81 mm.

The width of the wall deviates almost linearly from 0 to 2.17 mm. The total deviation is 37%. The thermal metric deviates in three phases. The first phase from layer 7 to 20 evolves slowly with a variation under 20%. Then a gap occurs, and deviation rises up to layer 30 from 20 to 25%. Finally, from layer 31, the thermal metric quickly rises with no tendency until a deviation of 176%.

3.1.2 Idle time of 30 s

The reference width is equal to 5.33 mm.

There is still a deviation of the width. This deviation is almost linear and reaches0.78 mm, a deviation of 14%. The thermal metric is stable for the first 22 layers. Then oscillations of its value are observed until the end of the wall. The thermal deviation reaches 20% for the layer 43.

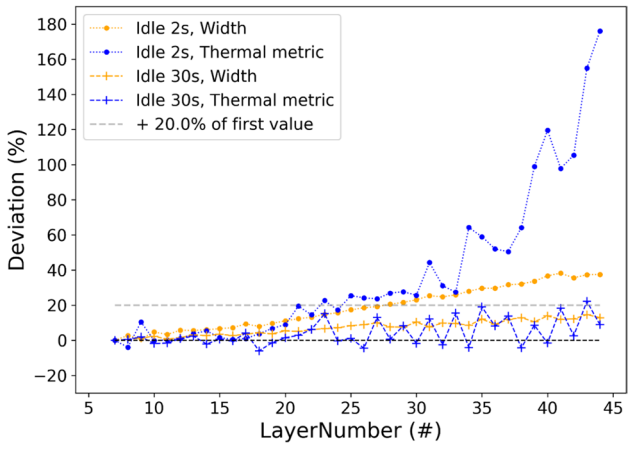

Fig. 12 Mean width deviation and mean normalized thermal metric as a function of the layer numberfor the two wall. For the 2-s idle time wall, the reference width is equal to 5.81 mm. For the 30-s idle time wall, the reference width is equal to 5.33 mm.

3.2 On the bead scale

In this part, all the data are kept, including those corresponding to the ends of the walls. The results are plotted for one layer. The deviation of the width and the thermal metric are calculated for each layer to the referent layer (layer 7) as in the previous part. Considering that the images are not synchronized with the robot, all the images in a layer are linearly distributed in function of the wall length.

3.2.1 Idle time of 2 s

The results for the layers 18 and 31 are presented in Fig. 13.

For these layers, two peaks of width deviation are observed at the ends of the wall. The deviations of the peaks are higher than 1 mm. The width deviations are stable in the middle of the wall, but the mean width is greater for the higher layer. One peak is observed for the thermal metric, at the beginning of the layer. The beginning of the layer is not the same in function of the manufacturing direction because of the zigzag strategy.

For the layer 18, the thermal reaches a pic at 1.4 of the normalized value, decreasing to the reference in the middle of the wall and remaining stable until the end of the layer. For the layer 31, the thermal metric reaches a peak at 2 of the normalized values and decreasing to the reference at the end of the layer. There is no constant value of the thermal metric.

3.2.2 Idle time of 30 s

The result of the layers 18 and 43 are presented in Fig. 14.

For these layers, two variations of width deviation are observed at the ends of the wall. The deviations are smaller than 1 mm. The width deviations are stable in the middle of the wall, but the mean width is higher for the layer 43. The thermal metric is stable in the layer 18. For the layer 43, an offset of the thermal metric is observed.

4 Discussion

4.1 On the wall scale

The results illustrate the correlation between the mean thermal metric and the mean width deviation. Indeed, the width deviates for both walls on each layer such as the thermal metric. However, the thermal metric seems to have a threshold value before deviating. For the wall made with an idle time of 2 s, the deviation appears at the layer 20. The thermal

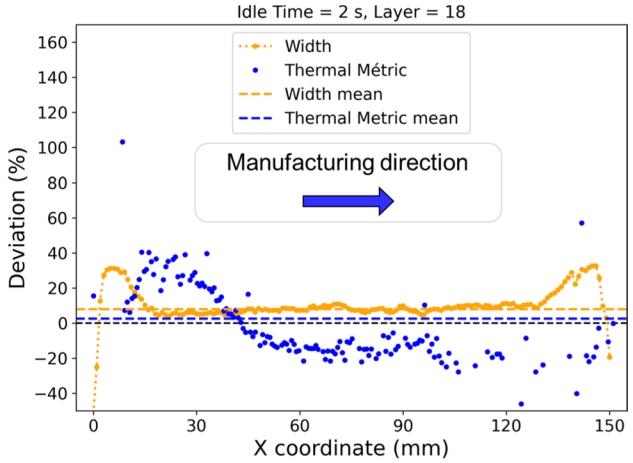

a) Layer 18, Idle time = 2s. Referent width is 5.81 mm

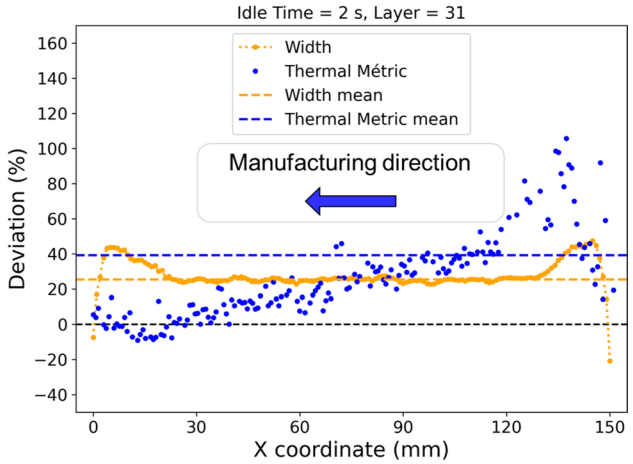

b) Layer 31, Idle time = 2s, Referent width is 5.81 mm

Fig. 13 Width deviation and mean normalized thermal metric function of the x-coordinate of the wall for a chosen layer and an idle time of 2 s

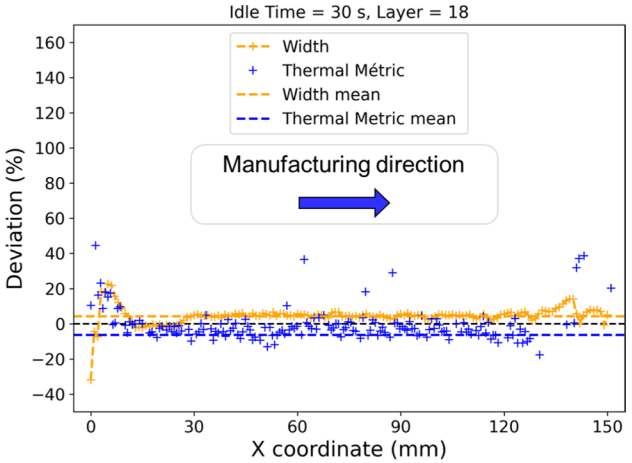

a) Layer 18, Idle time = 30s, Referent width is 5.33 mm

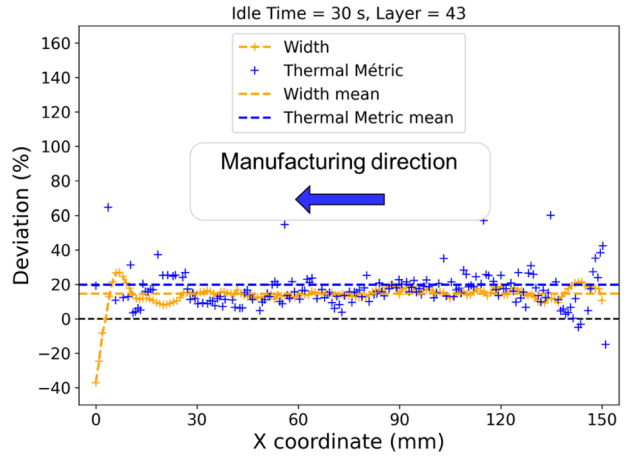

b) Layer 43, Idle time = 30s, Referent width is 5.33 mm

Fig. 14 Width deviation and mean normalized thermal metric function of the x-coordinate of the wall for a chosen layer and an idle time of 30 s

metric deviates above 20% of the referent value with a width deviation of 0.72 mm (12%). For the wall made with an idle time of 30 s, the deviation of the thermal metric above 20% is only reached before the last layer. The width deviation is equal to 0.78 mm (14%). The minimal deviation that can be observed by the method is a deviation of 20% of the thermal metric.

4.2 On the bead scale

For the four presented layers, the thermal metric is not noisy even if a simple image process has been used. The use of such a simple threshold to obtain the thermal processed area may be criticized, but results are stable.

For the idle time of 2 s, the global variation of the thermal metric can be explained by the zigzag strategy. Indeed, at the beginning of the layer, the deposition is done where the previous deposition finished a few seconds earlier. The idle time is too short to homogenize the temperature. A hot spot still remains when the torch comes back. For layer18, the thermal metric stabilization appears in the middle of the layer, whereas it appears at the end of layer 31, which illustrates the heat accumulation during the manufacturing process. It was shown previously when considering averaged thermal metrics over each layer. Concerning the thermal metric peak at each layer, a correlation is observed with one peak of width deviation. The other width deviation peakcomes from the previous and the next layer due to the zigzag strategy and the scan process method. Indeed, the variation of the width is measured by the scan after the manufacturing. The scan measures the global shape of the wall, and the scan is not able to get the geometry of a specific layer. Moreover, the

residual deformation of the wall may have an effect of the geometry, but it is ignored in this study. The second peak is an image of the peak from the previous and the next layers. A correlation between the first peak of the width and the thermal metric is proposed, and it illustrates the particular heat exchange at the end of the wall. Considering the history effect of the manufacturing seems to be necessary to monitor the defects.

For the wall made with an idle time of 30 s, at the opposite, the thermal metric is stable all along the length of the wall for both layers. The deviation observed is only an offset of the thermal metric. The idle time is long enough to obtain a homogenous temperature on the previous layer. The variation of the width deviation at the ends along the layer is below 1 mm. It is consistent with the results on the wall scale. They showed a sensitivity of the thermal metrics for width deviation above 1 mm.

The thermal behavior of the two walls is different. For the wall with an idle time of 30 s, there is only a phenomenon on the wall scale, whereas for the wall with an idle time of 2 s, there are phenomena on the scale of the wall and the bead. This difference can explain the differences between minimal quality deviations measured on the results on the wall scale.

Although a threshold for detecting a thermal deviation on the bead scale is delicate to define, the correlation between the deviation of the thermal metric and the width deviation is illustrated. The thermal metric sensibility could be improved by more advanced image process. These improvements could propose criteria for recording thermal deviation on the bead scale.

5 Conclusion and perspectives

This paper proposes a method to qualify the minimal geometrical deviation that can be measured with a CMOS camera in WAAM when manufacturing aluminum alloys. The literature highlights the complexity to extract the melt pool boundary from near-infrared camera images for aluminum alloy compared with steel. This article proposes to define a thermal metric: the surface of an area above a threshold after an image treatment. An experiment is done to show the correlation between this thermal metric and geometrical defects, here the width of a wall. Two different thermal conditions are tested by building two walls with different idle times. One wall is manufactured with an idle time of 2 s, inducing high heat accumulation; another wall is built with an idle time of 30 s, inducing little heat accumulation. The correlation between width and thermal metric deviations is demonstrated on the two walls. On the wall scale, considering the uncertainties, the minimal thermal metric deviation that can be detected is equal to 20% corresponding to a width deviation of 12%. On the bead scale, the analysis of the result points out the interest of the method and the complexity of the data analysis. This work demonstrates that the use of the near-infrared camera for monomodal monitoring of the thermal in WAAM aluminum is promising.

In this step, the method has been demonstrated with one geometrical defect (width of the wall). To reinforce this result, the potential of using a simple thermal deviation metric to monitor the global part quality could be illustrated with other defects such as porosities or residual stresses. Moreover, the sensitivity of the detection could be improved by a more optimized image processing. It may lead to a better qualification of the device on the scale of a bead. Finally, this method seems to be an encouraging solution for closed-loop control to manage heat accumulation during manufacturing and improve part quality.

Acknowledgements This work made use of the facilities of the platform S.mart Grenoble Alpes. The authors thank the staff of S.mart Grenoble Alpes, especially Devos Camille and Duong Quoc-Bao for their help on 0-V detection.

Author contributions All authors contributed to the study conception and design. Material preparation, data collection, and analysis were performed by Anthony Dellarre and Nicolas Béraud. The first draft of the manuscript was written by Anthony Dellarre, and all authors commented on previous versions of the manuscript. All authors read and approved the final version of the manuscript.

Funding This work benefited from the support of the project METALICANR-21-CE10-0003 of the French National Research Agency (ANR).

Declarations

Competing interests The authors declare no competing interests.

References

1. Xia C, Pan Z, Polden J et al (2020) A review on wire arc additive manufacturing: monitoring, control and a framework of automated system. J Manuf Syst 15. https://doi.org/10.1016/j.jmsy.2020.08.008
2. Ding D, Pan Z, Cuiuri D, Li H (2015) Wire-feed additive manufacturing of metal components: technologies, developments and future interests. Int J Adv Manuf Technol 81:465–481. https://doi.org/10.1007/s00170-015-7077-3
3. Chen X, Kong F, Fu Y et al (2021) A review on wire-arc additive manufacturing: typical defects, detection approaches, and multisensor data fusion-based model. Int J Adv Manuf Technol 117:707–727. https://doi.org/10.1007/s00170-021-07807-8
4. Rodríguez-González P, Ruiz-Navas EM, Gordo E (2023) Wire arc additive manufacturing (WAAM) for aluminum-lithium alloys: a review. Materials 16:1375. https://doi.org/10.3390/ma16041375
5. Béraud N, Chergui A, Limousin M et al (2022) An indicator of porosity through simulation of melt pool volume in aluminum wire arc additive manufacturing. Mech Ind 23:1. https://doi.org/10.1051/meca/2021052
6. Marinelli G, Martina F, Ganguly S, Williams S (2019) Development of wire + arc additive manufacturing for the production of

large-scale unalloyed tungsten components. Int J Refract Met Hard Mater 16. https://doi.org/10.1016/j.ijrmhm.2019.05.009
7. Ding J, Colegrove P, Mehnen J et al (2011) Thermo-mechanical analysis of wire and arc additive layer manufacturing process on large multi-layer parts. Comput Mater Sci 50:3315–3322. https://doi.org/10.1016/j.commatsci.2011.06.023
8. Sun J, Hensel J, Köhler M, Klaus D (2021) Residual stress in wire and arc additively manufactured aluminum components. J Manufac Process 65:97–111. https://doi.org/10.1016/j.jmapro.2021.02.021
9. Laghi V, Palermo M, Gasparini G et al (2019) Geometrical characterization of wire-and-arc additive manufactured steel element. Adv Mater Lett 10:695–699. https://doi.org/10.5185/amlett.2019.0019
10. Yildiz AS, Davut K, Koc B, Yilmaz O (2020) Wire arc additive manufacturing of high-strength low alloy steels: study of process parameters and their influence on the bead geometry and mechanical characteristics. Int J Adv Manuf Technol 108:3391–3404. https://doi.org/10.1007/s00170-020-05482-9
11. Tonelli L, Laghi V, Palermo M et al (2021) AA5083 (Al–Mg) plates produced by wire-and-arc additive manufacturing: effect of specimen orientation on microstructure and tensile properties. Prog Addit Manuf 6:479–494. https://doi.org/10.1007/s40964-021-00189-z
12. Wu B, Pan Z, Ding D et al (2018) A review of the wire arc additive manufacturing of metals: properties, defects and quality improvement. J Manuf Process 35:127–139. https://doi.org/10.1016/j.jmapro.2018.08.001
13. Köhler M, Hensel J, Dilger K (2020) Effects of thermal cycling on wire and arc additive manufacturing of Al-5356 components. Metals 10:952. https://doi.org/10.3390/met10070952
14. Bikas H, Stavropoulos P, Chryssolouris G (2016) Additive manufacturing methods and modelling approaches: a critical review. Int J Adv Manuf Technol 83:389–405. https://doi.org/10.1007/s00170-015-7576-2
15. Raghunath N, Pandey PM (2007) Improving accuracy through shrinkage modelling by using Taguchi method in selective laser sintering. Int J Mach ToolsManuf 47:985–995. https://doi.org/10.1016/j.ijmachtools.2006.07.001
16. Chergui A, Villeneuve F, Béraud N, Vignat F (2022) Thermal simulation of wire arc additive manufacturing: a new material deposition and heat input modelling. Int J Interact Des Manuf. https://doi.org/10.1007/s12008-021-00824-7
17. Stavropoulos P, Chantzis D, Doukas C et al (2013) Monitoring and control of manufacturing processes: a review. Procedia CIRP 8:421–425. https://doi.org/10.1016/j.procir.2013.06.127
18. Xu F, Dhokia V, Colegrove P et al (2018) Realisation of a multi-sensor framework for process monitoring of the wire arc additive manufacturing in producing Ti-6Al-4V parts. Int J Comput Integr Manuf 31:785–798. https://doi.org/10.1080/0951192X.2018.1466395
19. Davies GJ, Garland JG (1975) Solidification structures and properties of fusion welds. Int Metall Rev 20:83–108. https://doi.org/10.1179/imtlr.1975.20.1.83
20. Halisch C, Radel T, Tyralla D, Seefeld T (2020) Measuring the melt pool size in a wire arc additive manufacturing process using a high dynamic range two-colored pyrometric camera. Weld World 64:1349–1356. https://doi.org/10.1007/s40194-020-00892-5
21. García de la Yedra A, Pfleger M, Aramendi B et al (2019) Online cracking detection by means of optical techniques in laser-cladding process. Struct Control Health Monit 26:e2291. https://doi.org/10.1002/stc.2291
22. Xiong J, Lei Y, Chen H, Zhang G (2017) Fabrication of inclined thin-walled parts in multi-layer single-pass GMAW-based additive manufacturing with flat position deposition. J Mater Process Technol 240:397–403. https://doi.org/10.1016/j.jmatprotec.2016.10.019
23. Rouquette S, Cambon C, Bendaoud I, Soulié F (2020) Estimation of the heat source parameters during the deposition of SS316L wire with GMAW-CMT process: application to additive manufacturing. Société Française de Thermique. https://doi.org/10.25855/SFT2020-128
24. Dellarre A, Limousin M, Beraud N (2023) Melt pool acquisition using near-infrared camera in aluminum wire arc additive manufacturing. In: Gerbino S, Lanzotti A, Martorelli M et al (eds) Advances on Mechanics, Design Engineering and Manufacturing IV. Springer International Publishing, Cham, pp 803–814
25. Cambon C, Bendaoud I, Rouquette S, Soulié F (2022) A WAAM benchmark: from process parameters to thermal effects on weld pool shape, microstructure and residual stresses. Mater Today Commun 33:104235. https://doi.org/10.1016/j.mtcomm.2022.104235
26. Manokruang S, Vignat F, Museau M, Linousin M (2021) Model of weld beads geometry produced on surface temperatures by wire and arc additive manufacturing (WAAM). IOP Conf Ser: Mater Sci Eng 1063:012008. https://doi.org/10.1088/1757-899X/1063/1/012008
27. Montevecchi F, Venturini G, Grossi N et al (2018) Idle time selection for wire-arc additive manufacturing: a finite element-based technique. Addit Manuf 21:479–486. https://doi.org/10.1016/j.addma.2018.01.007
28. Bradski G, Kaehler A (2008) Learning OpenCV: computer vision with the OpenCV library. O'Reilly Media, Inc.
29. Dellarre A, Béraud N, Tardif N, Vignat F, Villeneuve F, Limousin M (2022) Qualify a near-infrared camera to detect thermaldeviation during aluminum alloy wire arc additive manufacturing. Recherche Data Gouv. https://doi.org/10.57745/7HF7KG